RESEARCH ARTICLE

American Journal of Botany

BRIEF COMMUNICATION

Peak values of twist-to-bend ratio in triangular flower stalks of *Carex pendula*: a study on biomechanics and functional morphology

Olga Speck[1,2,3,*], Feray Steinhart[1,*], and Thomas Speck[1,2]

Manuscript received 26 March 2020; revision accepted 12 June 2020.

[1] Plant Biomechanics Group, Botanic Garden, Faculty of Biology, University of Freiburg, Germany

[2] Cluster of Excellence *liv*MatS @ FIT Freiburg Center for Interactive Materials and Bioinspired Technologies, University of Freiburg, Germany

[3] Author for correspondence: (e-mail: olga.speck@biologie.uni-freiburg.de)

[*] Shared first authorship

Citation: Speck, O., F. Steinhart, and T. Speck. 2020. Peak values of twist-to-bend ratio in triangular flower stalks of *Carex pendula*: a study on biomechanics and functional morphology. *American Journal of Botany*. 107(11): 1588–1596.

doi:10.1002/ajb2.1558

PREMISE: Because of their own weight and additional wind forces, plants are exposed to various bending and torsional loads that sometimes require contradictory structural characteristics and mechanical properties. The resulting trade-off between flexural and torsional rigidity can be quantified and compared using the dimensionless twist-to-bend ratio.

METHODS: The flexural rigidity of the stems of *Carex pendula* was determined by 2-point bending tests. Additionally, 4-point bending tests and torsional tests were carried out on segments of two internodes directly below the inflorescences to measure flexural and torsional rigidity. Anatomical investigations were performed to quantify the cross-sectional distribution of their tissues.

RESULTS: The flexural rigidity of the stems, segments of the apical internode 1, and the more basal internode 2 differed significantly from each other, whereas the bending elastic moduli were not significantly different. The torsional rigidity of segments of internode 2 was a factor of 3.3 higher than that of internode 1, whereas the torsional moduli did not differ significantly. The twist-to-bend ratios of segments of internode 1 and 2 reached values between 85 and 403. Light microscopic investigations revealed a triangular stem possessing individual sclerenchyma strands, with internode 2 having significantly more strands than internode 1.

CONCLUSIONS: In the case of *Carex pendula*, flexural and torsional rigidity are adapted to the given mechanical constraints by significant changes in morphometric variables (axial and polar second moment of area, number of sclerenchyma strands), whereas the material properties (bending and torsional modulus) do not change markedly along the stem.

KEY WORDS bending elastic modulus; Cyperaceae; flexural rigidity; morphometry; torsional modulus; torsional rigidity; sclerenchyma; taper.

Plants have evolved markedly different body plans (= for plants also termed "bauplans"; Drost et al., 2017), but from a mechanical point of view, all plants are biological materials systems that are characterized, on the one hand, by anatomical heterogeneity caused by the specific three-dimensional arrangement of various tissues and, on the other hand, by mechanical anisotropy resulting from the various mechanical properties of the individual tissues. Despite these similarities, plants differ in their morphological features, anatomical characteristics, and mechanical properties as an adaptation to their habitat and as a response to changing environmental conditions that expose them to various and sometimes conflicting constraints. These constraints include various bending loads mainly caused by

American Journal of Botany 107(11): 1588–1596, 2020; http://www.wileyonlinelibrary.com/journal/AJB © 2020 The Authors. American Journal of Botany published by Wiley Periodicals LLC on behalf of Botanical Society of America. This is an open access article under the terms of the Creative Commons Attribution License, which permits use, distribution and reproduction in any medium, provided the original work is properly cited.

their own weight and wind and by torsional loads typically caused by wind (Ennos, 1993; Niklas, 1992, 1999). They counteract bending loads through high flexural rigidity and torsional loads through low torsional rigidity or in other words high torsional flexibility. Both flexural rigidity (*EI*) and torsional rigidity (*GJ*) are composite variables that combine material properties (bending modulus *E* and torsional modulus *G*) and morphometric variables (size and shape reflected by axial second moment of area *I* and polar second moment of area *J*). The bending and torsional modulus (SI unit: N m^{-2} or Pascal) define the relationship between stress (= applied force/unit area) and strain (= displacement/reference condition) as a measure for stiffness in the linear-elastic range. The axial and polar second moment of area (SI unit: m^4) are geometrical variables, which reflect how the points of a cross section are distributed in relation to a bending or torsional neutral plane or axis, respectively. In the context of a trade-off between flexural and torsional rigidity, the dimensionless twist-to-bend ratio (*EI*/*GJ*) is particularly interesting as it also provides information about the ratio of material properties (*E*/*G*) and morphometric variables (*I*/*J*) (Etnier, 2003; Vogel, 1992, Vogel, 2007).

With regard to morphology, the outer shape of the respective plant organ plays a major role in biomechanical performance. Etnier (2003) created a so-called stiffness mechanospace defined by values of flexural rigidity and torsional rigidity taking into account the cross-sectional shape and Poisson's ratio of plant axes. Ennos (1993) investigated the flexural rigidity and torsional rigidity along the triangular flower stalks of the lesser pond-sedge (*Carex acutiformis*) and found mean *EI*/*GJ* ratios of 36.0 ± 11.3, with the lowest ratios near the base of the flower stalk and the highest about halfway up the stalk before a reduction again toward the tip. The U-shaped cross sections of banana petioles (*Musa textilis*) with *EI*/*GJ* values ranging from 40 to 75 are among the highest values ever measured for plant axes (Ennos et al., 2000). Unpublished measurements of *Musa textilis* cross sections give a value of about 0.48 for *I*/*J*. Consequently, the bending elastic modulus is about 84 to 156 times higher than the torsional modulus. Comparable high *E*/*G* ratios have been found for petioles of *Musa acuminata* with values up to 124 and of *Ensete ventricosum* with values up to 81 (Ahlquist et al., 2015).

In this study on biomechanics and functional morphology of flower stalks of *Carex pendula*, we focused on (1) a comparison of the flexural rigidity of the flower stalk after removal of the most basal internode, leaves, and inflorescences and of individual internodal segments, (2) a comparison of the flexural rigidity and torsional rigidity and, thus, the twist-to-bend ratio of two adjacent internodes, and (3) the influence of the amount and arrangement of individual sclerenchyma strands on the mechanical performance of the internodes.

MATERIALS AND METHODS

Definitions

To avoid misunderstanding, we used the following definitions throughout the entire publication: flower stalk = stem with inflorescences, leaf blades, and leaf sheaths (Fig. 1B); stem = flower stalk without inflorescences, leaf blades, and sheaths, consisting of internodes and nodes, to be tested in 2-point bending (Fig. 1C); segment = part of the internode (Fig. 1D) to be tested in 4-point bending (Fig. 1E) or torsion; test sample = general term for all samples that have been tested or examined.

Plant material

Carex pendula Huds. is a perennial plant from the Cyperaceae family and forms large and dense tufts (Fig. 1A). To guarantee comparability of results, we collected all test samples from a single plant tuft (Fig. 1A), which was cultivated in the open field of the Botanic Garden of the University of Freiburg, Germany (latitude/longitude 48.008616/7.855774). To ensure that the flower stalks have the same developmental stage, we collected only those that had previously formed six mature inflorescences with comparable inflorescence mass and inflorescence length. The collections of plant materials took place within 14 days. The flower stalks were cut off near the base. A total of 15 test samples was analyzed in each mechanical test and anatomical examination. Leaf sheaths and leaf blades were removed before mechanical tests. For avoiding dehydration during the mechanical tests, the stems cut at the base were stored in water, and the cut surfaces of the internodes were sealed with petroleum jelly (Vaseline).

Morphometric data

Morphometric data were collected from individual test samples. The total stem length and the total length of the internodes were measured using a measuring tape with a millimeter graticule. Side length *s* and corresponding height *h* (Fig. 2A) were measured on all three sides of the cross section at various points along the respective test sample using a digital caliper (accuracy: ±0.01 mm). From these data, individual axial and polar second moments of area were calculated, respectively.

The axial second moment of area *I* of the triangular stems and segments was calculated using Eq. 1:

$$I = \frac{h^3 s}{36}. \quad (1)$$

The polar second moment of area *J* of the triangular segments was calculated using Eq. 2 (Richard and Sander, 2006):

$$J = \frac{4sh^3 + 3s^3 h}{114}. \quad (2)$$

(Note: We are fully aware that the torsional moment of area of an isosceles triangle calculates to $I_{\text{torsional}} = \frac{s^4}{46.2}$; i.e., it is 1.66 smaller than its polar second moment of area $I_{\text{pol}} = \frac{s^4}{27.7}$ used in our calculations. Since the cross-sectional shape of the flower stalk of *C. pendula* has strongly rounded corners and slightly outwardly curved flanks, its torsional behavior probably resembles a circular cross section more than a triangle with sharp corners and straight flanks; thus, we decided to use the polar second moment of area in our calculation.)

Two-point bending tests

The flexural rigidity *EI* of stems consisting of the apical three nodes (N_1–N_3) and two internodes (I_1 and I_2) was measured by means of two-point bending tests (Fig. 1C). The upper left edge of a vertically positioned plastic plate was glued horizontally to a piece of timber of square cross section to which internode 3

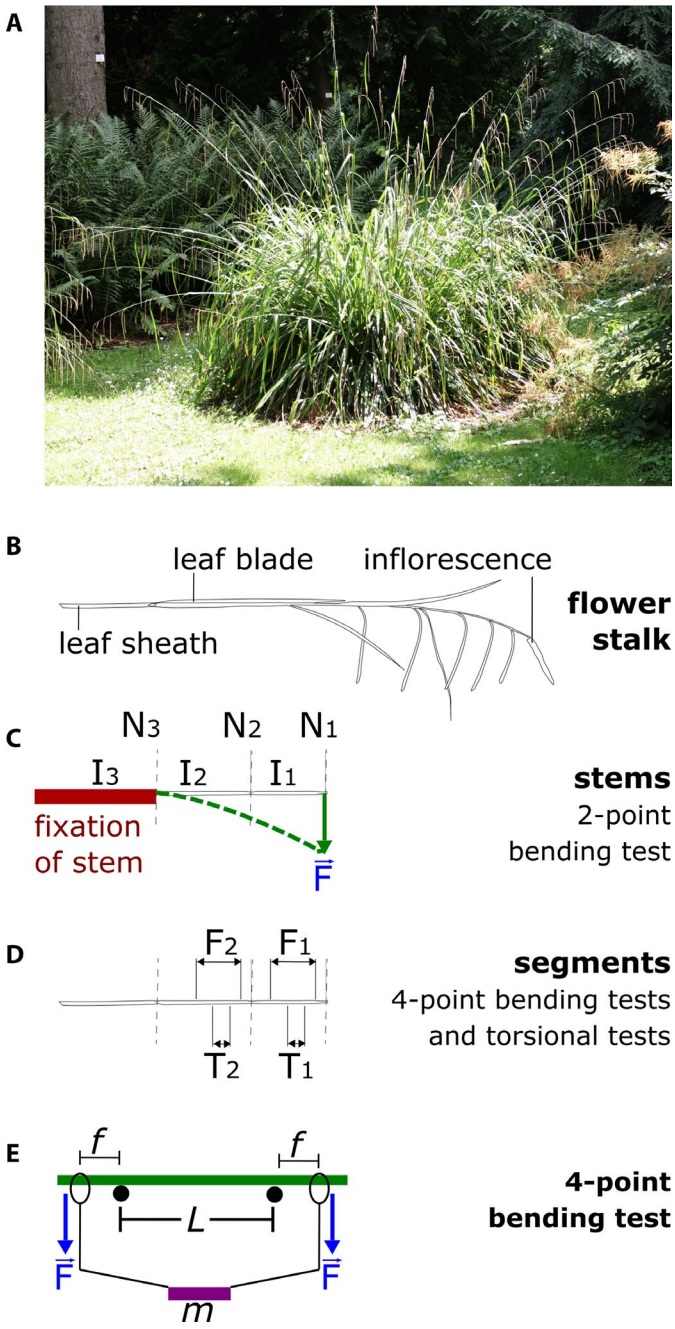


FIGURE 1. *Carex pendula*. (A) Dense tuft with long flower stalks in the Botanic Garden Freiburg, Germany. (B) Schematic drawing of a typical flower stalk with leaf blades, leaf sheaths, and inflorescences. (C) Two-point-bending tests were carried out on stems after removal of inflorescences, leaf blades, and leaf sheaths. The third internode I_3 was fixed horizontally to the piece of timber of square cross section (red). At the tip of the free-hanging stem, a total mass of up to 19 g was applied in cumulative steps (blue), and the respective displacement (green arrow) at the tip of the bent stem (dashed green line) was recorded. N1–N3 = nodes 1–3. (D) Four-point-bending tests were carried out on segments F_1 and F_2 from internodes I_1 and I_2, respectively. Directly after the bending tests, segments T_1 and T_2 were prepared for torsional tests. (E) Experimental setup of the four-point bending test. L (= 60 mm) is the distance between the center points of the central supports and f (= 15 mm) is the distance between the center point of one support and the center point of the corresponding arm of the mass holder (m).

of each stem was fixed with a screw clamp. A total of up to 19 g was applied to the tip of the free-hanging stem in cumulative steps beginning with 5 g and then in additive steps of 2 g. The respective displacement of the stem tip was plotted on graph paper attached to the plastic plate (accuracy: ±1 mm) at 60 s after application of a new weight. The flexural rigidity was calculated using Eq. 3, where E is the bending elastic modulus, L is the length of the stem between the support point and the attached mass, k is the slope in the displacement-force diagram, and I is the axial second moment of area:

$$EI = \frac{L^3}{3k}. \quad (3)$$

Four-point bending tests

From the stems previously used in the two-point bending tests, two segments (F_1 and F_2) were prepared from internodes I_1 and I_2, each segment lying 20 mm below the adjacent apical node and with a total length of 120 mm (Fig. 1C, D). The flexural rigidity of each segment was determined on all three sides, and then the average value was calculated. The four-point bending tests were performed using a custom-made steel-frame bending apparatus (Fig. 1E; Technical Workshop, Institute of Biology II/III, University of Freiburg, Germany). It consisted of two supports, a mass holder, and a microscope with an eyepiece graticule (accuracy: ±0.02 mm) to measure the displacement of the segments (Kaminski et al., 2017). The force was manually applied in cumulative steps, with a 60-s pause before the displacement was read, and the next weight was applied. Each triangular segment was bent within the linear-elastic range. The flexural rigidity was calculated by using Eq. 4 (Kaminski et al., 2017):

$$EI = \frac{L^2 f}{16k}, \quad (4)$$

where E is the bending elastic modulus, I is the axial second moment of area, L is the distance between the center points of the central supports (L = 60 mm), and f is the distance between the center point of one support and the center point of the corresponding holder arm (f = 15 mm). The respective slope of the regression line k was determined on the basis of the displacement-force curves.

Bending elastic modulus

From the flexural rigidity determined in two-point bending tests and four-point bending tests and the means of the individually calculated axial second moment of area, the bending elastic modulus E of the stems and segments was calculated using Eq. 5:

$$E = \frac{EI}{I}. \quad (5)$$

To take into account the taper of the stems, the tapering mode α was calculated from the regression line of a double logarithmic diagram with $\log z$ on the x-axis, where $z = x/L$ is the relative distance from the apical end, and $\log\left[\frac{r(x)-r_a}{r_b-r_a}\right]$ on the y-axis, where $r(x)$ is the equivalent

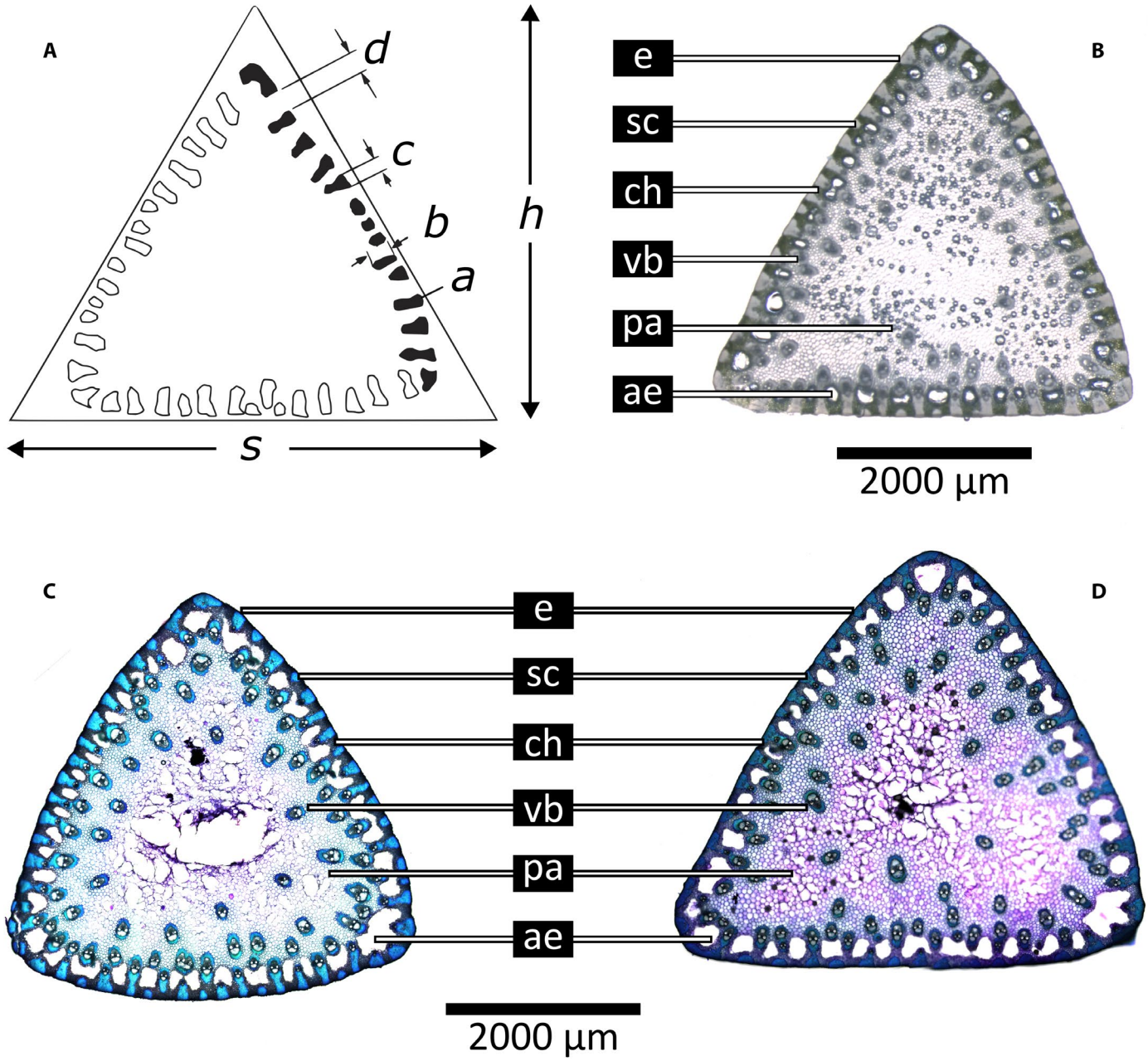


FIGURE 2. *Carex pendula*. (A) Schematic drawing of peripheral sclerenchyma strands (black) in the cross section. Morphometric variables: *a* area, *b* radial dimension, *c* tangential dimension, *d* distance between individual elements, *s* side length, *h* height. (B) Unstained handmade cross section of the more basal internode 2. Cross sections of (C) apical internode 1 and (D) more basal internode 2 stained with toluidine blue. Lignified cell walls of xylem and sclerenchyma appear blue-green, and unlignified cell walls of parenchyma and collenchyma are colored pinkish-purple. ae = aerenchyma, ch= chlorenchyma, e = epidermis, pa = parenchyma, sc = sclerenchyma, vb = vascular bundle.

radius at distance x from the base, r_b is the equivalent radius at the base and r_a is the equivalent radius at the apex of the stem (Caliaro et al., 2013). The bending elastic modulus E_{alpha} considering the tapering mode α was calculated according to Eq. 6, where L is the length of the stem between the support point and the attached mass, k is the slope in the displacement-force diagram and I_b is the axial second moment of area at the base (Caliaro et al., 2013):

$$E_{alpha} = \frac{L^3}{3I_b k}\left(\frac{r_b}{r_a}\right)^{\alpha}. \quad (6)$$

Torsional tests

Torsional rigidity GJ was measured directly after the above-described four-point bending tests had been carried out. A 50-mm-long segment (T_1 and T_2) was prepared from the middle of the segments F_1 and F_2, respectively (Fig. 1D), and subjected to a torsional test. The remaining 35 mm in an apical and basal direction was used in subsequent histological analysis. Tests were performed using a custom-made apparatus (Technical Workshop, Institute of Biology II/III, University of Freiburg, Germany) with a spring-loaded cylinder

to apply torque to the segment (see fig. 5: Gallenmüller et al., 2001). One end of the segment was clamped into a stationary holder, and the other was clamped to a torsional cylinder. The holders were 3D-printed with respect to the cross-sectional geometry of the segment. In cumulative 5 to 10 steps, the torsion cylinder was rotated up to 200° (accuracy: ±1°). Torsional rigidity was calculated from the slope of the linear regression line based on plots of the resulting angle (in rad) against the applied torque by using Eq. 7 (Kaminski et al., 2017):

$$GJ = \frac{L}{k}, \tag{7}$$

where G is the torsional modulus, J is the polar second moment of area, L is the free length of the tested segment between the clamps, and k is the slope of the regression line of the angle-torque curves. From the torsional rigidity and the means of the individually calculated polar second moments of area, the torsional modulus of the segments was calculated using Eq. 8 (Kaminski et al., 2017):

$$G = \frac{GJ}{J}. \tag{8}$$

Twist-to-bend ratio

Because bending and torsional tests were carried out consecutively on the same segment, the twist-to-bend ratio could be calculated for every single segment according to Eq. 9 (Vogel, 1992, 2007):

$$\text{twist-to-bend ratio} = \frac{EI}{GJ}. \tag{9}$$

Anatomy

Cross sections from the apical part of the segments were cut by hand with a razor blade. To identify the various tissue types, we analyzed and imaged unstained cross sections (Fig. 2B) with a stereomicroscope SZX7 (Olympus, Tokyo, Japan) and an Altra 20 camera (Olympus) and Cell^D 2.8 Software (Olympus Soft Imaging Solutions Deutschland GmbH, Hamburg, Germany). Further morphometric data of the cross sections (Fig. 2A) were determined by using the image analysis software ImageJ v. 1.45g and a Bamboo Fun Graphics Tablet (Wacom Europe GmbH, Krefeld, Germany).

Statistics

Raw data (Appendix S1) were recorded and analyzed with Microsoft (Redmond, WA, USA) Office Excel 2007. The statistical analysis and the box plots were conducted with Gnu R 3.5.0 (R Core Team, 2018). Data are either represented by mean values ± 1 SD or shown as median values with respective interquartile ranges (IQR). Shapiro's test was applied to check for normal distribution. For pairwise comparison of related data, the paired Wilcoxon signed rank test was used if the data were non-normally distributed, whereas the paired *t*-test was used if the data were normally distributed. A two-way repeated measures (rm) ANOVA (normally distributed data) or Friedman rank sum test (non-normally distributed data) was applied to check for differences in flexural rigidity, bending elastic modulus, and morphometric data of the three sides of the triangular cross section (Appendix S2). Levels of significance were $P > 0.05$: not significant (n.s.); $P \leq 0.05$: significant (*); $P \leq 0.01$: very significant (**); $P \leq 0.001$: highly significant (***).

RESULTS

Bending tests

Table 1 summarizes the morphometric data and mechanical properties of the stems and segments and presents the statistical results. For seven of the 15 stems, the bending tests were performed on all three sides. The two-way rm-ANOVA showed that neither the flexural rigidity nor the bending elastic modulus E and E_{alpha} of the three sides differed significantly (Appendix S2). Based on this result, the remaining eight stems were tested on one side only. Statistical analyses showed that the data for flexural rigidity EI and the bending elastic modulus E were normally distributed, whereas E_{alpha} data were not normally distributed on one side. The tapering mode α of the stems (n = 14) yielded a median of 1.39 (IQR: 0.30). Using Eq. 6, we calculated the bending elastic modulus E_{alpha}, with a median of 13.71 GPa (IQR: 5.27 GPa). Although the median of E_{alpha} amounts to 88% of E with a median of 15.62 GPa (IQR: 4.12 GPa, E is calculated with the mean of the axial second moments of area measured along the stem), a paired *t*-test revealed that they did not differ significantly (t = 0.86338, df = 13, P = 0.4036). Comparisons of the stem with F_1, the stem with F_2, and F_1 with F_2, yielded highly significant differences for the flexural rigidity and the axial second moment of area, whereas no significant differences could be found for the bending elastic modulus (Table 1).

Torsional tests

Statistical analyses showed that data for the torsional rigidity, polar second moment of area, and torsional modulus were normally distributed. A comparison of T_1 and T_2 yielded highly significant differences for the torsional rigidity and the polar second moment of area, whereas no significant differences were found for the torsional modulus (Table 1).

Twist-to-bend ratio

Since the data for the twist-to-bend ratio of internode 1 were normally distributed, but that of internode 2 was not, a paired Wilcoxon signed rank test was performed. No significant differences were found (Table 1).

Morphology and anatomy

The flower stalks of *C. pendula* are divided longitudinally into internodes and nodes with inflorescences borne on long, drooping stalks. Light microscopic investigations showed a triangular cross section with rounded corners. In the periphery, alternating individual elements of various sizes consisted of lignified sclerenchyma fibers, chlorenchyma, and aerenchyma. As a characteristic for monocotyledons, the vascular bundles were in the form of an atactostele scattered throughout the parenchyma (Fig. 2).

For seven of the 15 cross sections, the morphometric data were analyzed on all three sides according to Fig. 2A. The two-way rm-ANOVA or a Friedman test showed that none of the measured

TABLE 1. Morphometric data and biomechanical properties of flower stalk, stems, and internodal segments of *Carex pendula*. Median values (Med) with interquartile ranges (IQR), minima (Min) and maxima (Max), sample sizes (*n*) for each variable, and the statistical results of the [1] paired *t*-test and [2] paired Wilcoxon signed rank test are given.

Variable	Sample	Med	IQR	Min	Max	*n* / Statistics
Length (mm)	Flower stalk	1340	106	1092	1542	$n = 15$
	Internode 1	275.0	37.8	209.5	360.0	$n = 15$
	Internode 2	320.0	30.5	245.0	425.0	$n = 15$
	Inflorescence	579.0	67.0	456.0	690.0	$n = 15$
Top load (g)	Inflorescence	3.85	1.10	2.02	4.79	$n = 15$
Flexural rigidity (***EI***)	Stem ($N\,m^2 \times 10^{-6}$)	94,325	36,475	51,000	133,377	$n = 15$
	F_1 ($N\,m^2 \times 10^{-6}$)	43,548	24,993	18,564	75,318	$n = 15$
	F_2 ($N\,m^2 \times 10^{-6}$)	142,529	90,245	64,564	288,431	$n = 15$
	Stem – F_1		$t = 13.103$, df = 14, $P = 3.056 \times 10^{-9}$			[1] ***
	Stem – F_2		$t = -4.659$, df = 14, $P = 3.687 \times 10^{-4}$			[1] ***
	F_1 – F_2		$t = -7.9912$, df = 14, $P = 1.387 \times 10^{-6}$			[1] ***
Axial second moment of area (***I***)	Stem (mm^4)	6.78	4.09	3.02	9.71	$n = 15$
	F_1 (mm^4)	2.73	1.13	1.33	4.19	$n = 15$
	F_2 (mm^4)	9.50	5.57	3.79	14.70	$n = 15$
	Stem – F_1		$t = 9.5906$, df = 14, $P = 1.564 \times 10^{-7}$			[1] ***
	Stem – F_2		$t = -5.5255$, df = 14, $P = 7.475 \times 10^{-5}$			[1] ***
	F_1 – F_2		$t = -8.8282$, df = 14, $P = 4.273 \times 10^{-7}$			[1] ***
Bending elastic modulus (***E***)	Stem (GPa)	15.62	4.12	11.04	19.52	$n = 15$
	F_1 (GPa)	16.60	2.36	12.65	20.98	$n = 15$
	F_2 (GPa)	16.20	4.42	9.76	21.71	$n = 15$
	Stem – F_1		$t = -1.5837$, df = 14, $P = 0.1356$			[1] n.s.
	Stem – F_2		$t = -0.8135$, df = 14, $P = 0.4296$			[1] n.s.
	F_1 – F_2		$t = 0.50272$, df = 14, $P = 0.623$			[1] n.s.
Torsional rigidity (***GJ***)	T_1 ($N\,m^2 \times 10^{-6}$)	222	114	89	516	$n = 15$
	T_2 ($N\,m^2 \times 10^{-6}$)	738	399	205	1581	$n = 15$
	T_1 – T_2		$t = -7.2135$, df = 14, $P = 4.47 \times 10^{-6}$			[1] ***
Polar second moment of area (***J***)	T_1 (mm^4)	6.33	3.82	2.67	10.54	$n = 15$
	T_2 (mm^4)	21.97	12.18	9.48	38.00	$n = 15$
	T_1 – T_2		$t = -8.7591$, df = 14, $P = 4.695 \times 10^{-7}$			[1] ***
Torsional modulus (***G***)	T_1 (MPa)	37.05	15.52	21.53	68.67	$n = 15$
	T_2 (MPa)	38.32	19.57	20.82	56.10	$n = 15$
	T_1 – T_2		$t = 0.82031$, df = 14, $P = 0.4258$			[1] n.s.
Twist-to-bend ratio	F_1/T_1	179	71	98	319	$n = 15$
	F_2/T_2	178	78	85	403	$n = 15$
	F_1/T_1 – F_2/T_2		$V = 58$, $P = 0.9341$			[2] n.s.

Note: flower stalk = stem with inflorescences, leaf blades, and leaf sheaths; stem = flower stalk without inflorescences, leaf blades, and sheaths, consisting of internodes and nodes; segment = part of internode 1 and 2 to be tested in bending (F_1 and F_2) or torsion (T_1 and T_2)

variables differed significantly when the interaction effect of test sample and side was taken into account (Appendix S2). Based on this result, the morphometric data of the remaining eight test samples were measured on one side only. Table 2 summarizes the morphometric data and presents the statistical results. Significant differences were found when comparing the numbers of sclerenchyma strands, whereas the area, radial, and tangential dimension of the sclerenchyma strands and the distance between each other did not differ significantly.

DISCUSSION

The literature on plant biomechanics demonstrates that both the cross-sectional shape in the form of the I/J ratio and the mechanical properties in the form of the E/G ratio determine the flexural and torsional rigidity and thus ultimately also the twist-to-bend ratio (Ennos et al., 2000; Kaminski et al., 2017; Niklas, 1992, 1999; Vogel, 1992). In general, quotients of the axial and polar second moment of area (I/J) are 0.2 to 0.5 for axes with U-shaped cross sections (unpublished data), 0.25 for elliptical cross sections if the minor axis is twice the major axis, 0.5 for circular cross sections, 0.81 for squared cross sections, 0.83 for isosceles triangles, and 1.25 for elliptical cross sections if the major axis is twice the minor axis (Niklas, 1999). Since I/J ratios are usually below 1.0, high twist-to-bend ratios must therefore be attributed to high E/G ratios, whereby these mechanical properties are essentially determined at the tissue level by the relationship $E \gg G$ (Niklas, 1999) and at the organ level by the 3D distribution of strengthening tissues within the parenchymatous matrix.

Average twist-to-bend ratios are 13.3 ± 1.0 for lenticular and hollow flower stalks of daffodils (*Narcissus pseudonarcissus*) (Etnier, 2003), 14.1 ± 4.1 for the circular-shaped petioles of the UFO plant (*Pilea peperomioides*) taking into account their tapering (Kelbel, 2019), 17.2 ± 7.8 for the square-shaped stems of motherwort (*Leonurus cardiaca*) (Kaminski et al., 2017), and 36.0 ± 11.3 for the triangular flower stalks of the lesser pond-sedge (*Carex acutiformis*) (calculated using data from Ennos, 1993). Of note, the peak values

TABLE 2. Morphometric data of the sclerenchyma strands in the internodes of *C. pendula*. Median values (Med) with interquartile ranges (IQR), minima (Min), and maxima (Max), the sample sizes (*n*) for each variable, and the statistical results of the [1] paired *t*-test and [2] paired Wilcoxon signed rank test are given.

Variable	Sample	Med	IQR	Min	Max	*n* / Statistics
Number / side						
	I_1	14	2.5	12	17	$n = 15$
	I_2	19	1.0	17	21	$n = 15$
	$I_1 - I_2$	$t = -10.132$, df = 14, $P = 7.934 \times 10^{-8}$				[1] ***
Area (***a***)						
	I_1 (mm^2)	0.0199	0.0054	0.0084	0.0283	$n = 15$
	I_2 (mm^2)	0.0209	0.0187	0.0059	0.0404	$n = 15$
	$I_1 - I_2$	$t = -0.50194$, df = 14, $P = 0.6235$				[1] n.s.
Radial dimension (***b***)						
	I_1 (mm)	0.1470	0.0442	0.1086	0.2235	$n = 15$
	I_2 (mm)	0.1731	0.0760	0.0749	0.2268	$n = 15$
	$I_1 - I_2$	$t = -0.75501$, df = 14, $P = 0.4628$				[1] n.s.
Tangential dimension (***c***)						
	I_1 (mm)	0.1190	0.0259	0.0823	0.1431	$n = 15$
	I_2 (mm)	0.1238	0.0425	0.0755	0.2433	$n = 15$
	$I_1 - I_2$	$t = -1.7968$, df = 14, $P = 0.09397$				[1] n.s.
Distance (***d***)						
	I_1 (mm)	0.1357	0.0302	0.0923	0.2361	$n = 15$
	I_2 (mm)	0.1778	0.0659	0.0687	0.2176	$n = 15$
	$I_1 - I_2$	$V = 38$, $P = 0.2293$				[2] n.s.

presented here for the triangular flower stalk of *Carex pendula* with mean values of 191 ± 70 for the two apical internodes exceed the highest values of approximately 75 measured for the U-shaped petioles of banana (*Musa textilis*) (Ennos et al., 2000).

The presented figures show that the very high values of the twist-to-bend ratios of *C. pendula* cannot be attributed to the triangular shape of the segments, which in this case has an average I/J ratio of 0.42 ± 0.05, but indicate the dominant contribution of the ratio of E/G of 465 ± 184. Interestingly, the bending elastic modulus and torsional modulus themselves do not vary significantly along the stem, but the significant differences in bending and torsional rigidity along the stalk result from changes in the axial and polar second moment of area, whereas the twist-to-bend ratios remain very high in each segment.

Our data support previous results suggesting that the inner stem structure plays a major role in terms of the three-dimensional arrangement of strengthening tissues. In the case of *N. pseudonarcissus*, which shows a rather low twist-to-bend ratio of 13.3 ± 1.0 despite having an elliptical flower stalk cross section, the vascular bundles are scattered throughout the flower stalk in the form of an atactostele, which is typical for monocotyledons. In comparison, dicotyledonous plant axes with peripherally arranged strengthening tissues such as the collenchyma, sclerenchyma, and xylem at the corners of the squared cross sections of *L. cardiaca* show markedly higher values for the twist-to-bend ratio of 36.0 ± 11.3 (Kaminski et al., 2017). The genus *Carex*, which belongs to the monocotyledons, has not only an atactostele, but also peripherally arranged sclerenchyma strands. The individual internodes of *C. pendula* differ highly significantly in the number of sclerenchyma strands but have a comparable area, radial and tangential dimension, and distance from each other. In addition to a high flexural rigidity, the *Carex* internodes have a high torsional flexibility, which is based on the isolation of the individual sclerenchyma strands by intervening chlorenchyma and aerenchyma, the latter creating space for torsional movement, especially in the three corners because of its mechanical compliance.

At this point, the influence of the nodes on the biomechanics of the flower stalk of the *C. pendula* should be discussed. Interestingly, the cross-sectional anatomy of the nodes is basically the same as for the internodes. In contrast to the internodes, the outer 2/3 of the nodes represents a strengthening ring that consists of a peripheral continuous ring of sclerenchyma without intervening aerenchym followed by vascular bundles of different size embedded in chlorenchyma. The central pith of unlignified parenchyma occupies only about 1/3 of the total area. A thin, continuous, lignified cell layer is conspicuous at the transition between the closely spaced vascular bundles and the unlignified parenchymatous pith. From a biomechanical point of view, the broader peripheral ring of strengthening tissues generally increases the flexural and torsional rigidity by increasing the axial and polar second moment of area. The above-described structure of the nodes, which differs from the internodes, may explain why the flexural rigidity of the stems consisting of two internodes and three nodes differs highly significantly from the flexural rigidity of the internodal segments. Additionally, the closed ring of sclerenchyma without intervening aerenchym especially increases the torsional rigidity of the nodes in contrast to the internodes with individual sclerenchyma strands alternating with aerenchymatous regions that allows for easier torsional movement (Wolff-Vorbeck et al., 2019).

In a comparison of *C. acutiformis* and *C. pendula*, which have the same body plan consisting of triangular flower stalks with internodes and nodes and a similar internal structure, the internodes of *C. pendula* have on average a 5.8–18.4 times higher flexural rigidity and a 1.1–3.5 times higher torsional rigidity than the mean values published for the stalk segments of *C. acutiformis* (calculated using data from Ennos, 1993). These values lead to an approximately 5-fold higher twist-to-bend ratio of the internodes of the larger *C. pendula* ranging between 98 and 403. *Carex pendula* flower stalks have a maximum length of 250 cm and carry an average inflorescence mass of 3.61 ± 0.80 g, which is a considerably higher top load than those of *C. acutiformis,* which carry an inflorescence mass of 0.92 ± 0.26 g (calculated using data from Ennos, 1993) on a maximum 150 cm long flower stalk. Calculating the bending moment as a product of lever arm and weight force from these values results in a bending moment 6.5 times higher for *C. pendula* than for *C. acutifomis;* a value which is in good agreement with the at least 5.8 times higher flexural rigidity of *C. pendula* stems. In addition, the two species differ in their growth form. *C. acutiformis* is an upright-growing plant with straight nearly vertical inflorescences. In contrast, *C. pendula* is an upright-growing plant, whose flower stalks are already (slightly) bent by the weight of its drooping inflorescences. Silk et al. (1982) introduced the interesting aspect of tapered axis into this discussion. Because of the taper, there is a lower flexural rigidity at the tip, which leads to a bending of the axis and thereby to a reduction of the moment arm produced by the top load.

However, the investigations of internode 1 and 2 of *C. pendula* only provide part of the mechanical characterization of the flower stalk. Likewise, the stem tested in two-point bending, after subtraction of inflorescences, leaves and basal internode 3, represents on average merely a section between 10.9 ± 6.1% and 56.1 ± 3.5% in relation to the total length (= 100%) of the flower stalk. In addition, more than half of each internode is surrounded in its basal

part by a leaf sheath consisting of a closed triangular ring, which completely surrounds the internode and is tight-fitting but not firmly grown together. In principle, the leaf sheath is made up of the same tissue layers as the flower stalk, but its broad peripheral sclerenchyma layer is particularly striking, taking up almost half of the ring diameter. Thus, the leaf sheath not only can give the internode additional flexural rigidity, but also allows free torsion within the leaf sheath and therefore has little influence on the torsional stiffness. Consequently, if the leaf sheath is included, the twist-to-bend ratio may reach even higher values than the peak values measured for the internodal segments alone. Furthermore, in the inflorescence region, the internode is no longer completely triangular. Usually, within the leaf sheath, the stalk of the respective inflorescence displaces one corner of the internode. Not all of these aspects of the overall flower stalk could be taken into account in the present study.

Another aspect we considered is the influence of the taper of the stems on the bending elastic modulus. The tapering mode α describes whether the shape resembles more a circular cylinder ($\alpha = 0$), a second order paraboloid of revolution ($\alpha = 0.5$), a circular cone ($\alpha = 1$) or a hyperboloid of revolution ($\alpha = 1.5$) (Caliaro et al., 2013). Depending on the respective taper, the difference of the elastic bending modulus can be more or less pronounced, if taking into account the mean values of the axial second moment of area or a—due to the tapering—apically decreasing axial second moment of area. For petioles of *Caladium bicolor* 'Candyland', a tapering mode of 0.37 was found. Thus, the bending elastic modulus considering the taper increased to 118% of the value without taper (Caliaro et al., 2011). In the case of *C. pendula*, the mean tapering mode is 1.37 ± 0.24, resulting in a median of E_{alpha} reduced to 88% compared to the bending elastic modulus E calculated from the mean of the individually calculated axial second moments of area.

A high twist-to-bend ratio of the flower stalk is a functional advantage, especially under wind loads. Despite its own weight and the additional top load of inflorescences and fruits, the flower stalk grows largely upright, and the wind-pollinated inflorescences extend far beyond the tuft of leaves. Additionally, the high torsional flexibility of the sagging flower stalk contributes to a turning out of the wind and thus to the avoidance of excessive forces and ultimately to damage prevention. Since plants are always the result of the respective body plan, a multifunctional structure and the response and adaptation to sometimes contradictory environmental and mechanical requirements, a quantitative analysis of the contributions made by the cross-sectional shape and internal structure of plant stems can only be achieved by simulations, in which the individual variables can be varied independently.

CONCLUSIONS

In the case of *Carex pendula* flower stalks, the increase in flexural rigidity and torsional rigidity from the more apical segment from internode I_1 to the more basal segment from internode I_2 is caused by morphological variables, i.e., a significant increase in axial and polar second moment of area, and by anatomical variables, i.e., a significant increase in the number of peripheral sclerenchyma strands, whereas the material properties (bending and torsional modulus) do not change markedly along the stem. The very high twist-to-bend ratio found in both internodal segments is partly attributable to the triangular shape of the stem but is mainly a consequence of a high bending modulus and a low torsional modulus causing an ecologically advantageous flexurally stiff but very torsional flexible flower stalk. This inspiring concept of nature might also be of relevance for implementation in slim technical constructions.

ACKNOWLEDGMENTS

We thank Ruwen Kaminski for his support during the practical work. Sandra Caliaro and Max Langer are gratefully acknowledged for preparing the stained sections. We thank Dr. R. Theresa Jones for improving the English. We are very grateful to two anonymous reviewers for their valuable comments, which have greatly improved this manuscript.

AUTHOR CONTRIBUTIONS

F.S. and O.S. conceived the study design. F.S. carried out the experiments. All authors analyzed and discussed the data. F.S. and O.S. performed the statistical analyses. O.S. wrote the first draft of the manuscript. All authors contributed significantly to the intellectual content of the final draft by interpreting and discussing the experimental data, revised the article, approved the final version of the manuscript, and agree to be held responsible for the content therein.

COMPETING INTERESTS

The authors declare no competing interests.

FUNDING INFORMATION

Partly funded by the Deutsche Forschungsgemeinschaft (DFG, German Research Foundation) under Germany's Excellence Strategy – EXC-2193/1 – 390951807 and Ministry of Science, Research, and the Arts of the Federal State of Baden-Württemberg in the framework of BioElast. The article processing charge was funded in the framework of the DEAL contract.

DATA AVAILABILITY

All relevant data are given within the paper and its electronic supplementary material.

SUPPORTING INFORMATION

Additional Supporting Information may be found online in the supporting information tab for this article.

APPENDIX S1. Raw data.

APPENDIX S2. A two-way repeated measures ANOVA or a Friedman rank sum test was performed to establish whether the three sides of the respective test sample differed significantly.

LITERATURE CITED

Ahlquist, S., T. Kampowski, O. O. Torghabehi, A. Menges, and T. Speck. 2015. Development of a digital framework for the computation of complex material and morphological behavior of biological and technological systems. *Computer-Aided Design* 60: 84–104.

Caliaro, M., F. Schmich, T. Speck, and O. Speck. 2013. Effect of drought stress on bending stiffness in petioles of *Caladium bicolor* (Araceae). *American Journal of Botany* 100: 2141–2148.

Caliaro, M., T. Speck, and O. Speck. 2011. „Smart Materials" – adaptive, pflanzliche Strukturen als Ideengeber für innovative, technische Verbundmaterialien mit steuerbarer Form- und Steifigkeitsregulation. In A. B. Kesel and D. Zehren (eds.), Bionik: Patente aus der Natur. Tagungsbeiträge zum 5. Bionik-Kongress in Bremen, 194–199. Bionik-Innovations-Centrum (B-I-C), Bremen, Germany.

Drost, H. G., P. Janitza, I. Grosse, and M. Quint. 2017. Cross-kingdom comparison of the developmental hourglass. *Current Opinion in Genetics & Development* 45: 69–75.

Ennos, A. R. 1993. The mechanics of the flower stem of the sedge *Carex acutiformis*. *Annals of Botany* 72: 123–127.

Ennos, A. R., H. Spatz, and T. Speck. 2000. The functional morphology of the petioles of the banana, *Musa textilis*. *Journal of Experimental Botany* 51: 2085–2093.

Etnier, S. A. 2003. Twisting and bending of biological beams: distribution of biological beams in a stiffness mechanospace. *Biological Bulletin* 205: 36–46.

Gallenmüller, F., U. Müller, N. Rowe, and T. Speck. 2001. The growth form of *Croton pullei* (Euphorbiaceae)—Functional morphology and biomechanics of a neotropical liana. *Plant Biology* 3: 50–61.

Kaminski, R., T. Speck, and O. Speck. 2017. Adaptive spatiotemporal changes in morphology, anatomy, and mechanics during the ontogeny of subshrubs with square-shaped stems. *American Journal of Botany* 104: 1157–1167.

Kelbel, M. C. 2019. Vergleichende Analyse stabförmiger biologischer Strukturen – Morphologie, Anatomie und Mechanik unter Biege- und Torsionslast. Bachelor's thesis, University Freiburg, Germany.

Niklas, K. J. 1992. Plant biomechanics: an engineering approach to plant form and function. University of Chicago Press, Chicago, IL, USA.

Niklas, K. J. 1999. A mechanical perspective on foliage leaf form and function. *New Phytologist* 143: 19–31.

R Core Team. 2018. R: A language and environment for statistical computing. R Foundation for Statistical Computing, Vienna, Austria. Website: https://www.R-project.org/.

Richard, H. A., and M. Sander. 2006. Technische Mechanik Festigkeitslehre. Vieweg Fachbücher der Technik, Wiesbaden, Germany.

Silk, W. K., L. L. Wang, and R. E. Cleland. 1982. Mechanical properties of the rice panicle. *Plant Physiology* 70: 460–464.

Vogel, S. 1992. Twist-to-bend ratios and cross-sectional shapes of petioles and stems. *Journal of Experimental Botany* 43: 1527–1532.

Vogel, S. 2007. Living in a physical world XI. To twist or bend when stressed. *Journal of Biosciences* 32: 643–655.

Wolff-Vorbeck, S., M. Langer, O. Speck, T. Speck, and P. Dondl. 2019. Twist-to-bend ratio: an important selective factor for many rod-shaped biological structures. *Scientific Reports* 9: 17182.